Rheology and Microrheology of Semiflexible Polymer Solutions: Actin Filament Networks

ARTICLE *in* MACROMOLECULES · SEPTEMBER 1998

Impact Factor: 5.8 · DOI: 10.1021/ma9717754

3 AUTHORS, INCLUDING:

Denis Wirtz
Johns Hopkins University
224 PUBLICATIONS **10,315** CITATIONS

SEE PROFILE

Rheology and Microrheology of Semiflexible Polymer Solutions: Actin Filament Networks

Jingyuan Xu, Andre Palmer, and Denis Wirtz*

Department of Chemical Engineering, The Johns Hopkins University, 3400 North Charles Street, Baltimore, Maryland 21218

Received December 5, 1997; Revised Manuscript Received July 16, 1998

ABSTRACT: We report a systematic study of the linear rheology of solutions of model semiflexible polymers, actin filaments (F-actin), using mechanical rheometry, diffusing wave spectroscopy (DWS), and video-based single-particle tracking microrheology. For pure actin at $c = 24$ μM and after full polymerization, the elastic and loss moduli still increase with time as $G'(t) \propto t^{0.25\pm0.02}$ and $G''(t) \propto t^{0.15\pm0.03}$, when measured at 1 rad/s, during network formation and reach a plateau after 12 h. At equilibrium, the linear small-frequency elastic modulus has a small magnitude, $G'_p = 14 \pm 3$ dynes/cm^2. The magnitude of G'_p depends weakly on concentration as $G'_p(c) \propto c^{1.2\pm0.2}$, with an exponent much smaller than for flexible polymers. At large concentrations, F-actin network becomes a liquid crystal and G'_p is independent of concentration. Using the large bandwidth of DWS, we show that the high-frequency viscoelastic modulus of F-actin solutions varies with the shear frequency as $|G^*(\omega)| \propto \omega^{0.78\pm0.10}$ for both the isotropic phase and liquid crystalline phase. These results are in good agreement with a recent model of semiflexible polymer solutions (the "curvature-stress" model) and reflect the finite rigidity of F-actin.

1. Introduction

Globular actin (G-actin) is a four-lobed protein in a low ionic strength buffer, which, in the presence of physiological concentrations of cations such as K^+ and/or Mg^{2+}, self-assembles into long filaments (F-actin).[1] In vitro and in the absence of capping proteins, the contour length of F-actin, $L \cong 1-20$ μm,[2] is larger than its persistence length, $L_p \cong 0.5-15$ μm, which is itself much larger than the polymer diameter, $d = 7$ nm.[3,4] Therefore, F-actin is considered to be a semiflexible polymer.[3,4] While solutions of flexible and rigid polymers have been extensively studied from both experimental and theoretical points of view,[5−8] only recently have theoreticians developed models that specifically describe the rheology of semidilute solutions of semiflexible polymers, such as F-actin solutions. These theories, that of MacKintosh et al.,[9] Isambert and Maggs,[10] and Morse[11] differ greatly in their predictions. In particular, these models offer vastly different predictions for the concentration dependence and the magnitude of the plateau modulus displayed by actin filament networks at low frequencies.

These models consider different origins for the elasticity of semiflexible polymer solutions at small frequencies. Isambert and Maggs,[10] and Morse[11] assume that the plateau modulus of a network of semiflexible polymers originate from the forces that prevent transversal fluctuations of the tube formed by the surrounding actin filaments (the curvature-stress model). MacKintosh et al.,[9] instead, assumes that the elasticity emanates from polymers being prevented to slide tangentially (the tension-stress model). The combination of vastly different values of the small-frequency elastic modulus G'_p[12−28] reported in the literature and the lack of a complete rheological data set have not provided theoreticians with a firm basis for a meaningful and rigorous test of their theories.

* Corresponding author. Fax: (410) 516-5510. Telephone: (410) 516-7006. E-mail: wirtz@jhu.edu.

This paper offers the first systematic study of pure-actin rheology: we report loss and storage moduli over extended ranges of oscillatory shear frequency (10^{-3} Hz $< \omega < 10^5$ Hz) and actin concentration (10 μM $< c <$ 164 μM). This paper uses novel advancements in actin preparation, which avoid some of the earlier pitfalls. In particular, we use gel-filtrated, nonfrozen, fresh actin, with negligible amounts of cross-linking proteins and capping proteins.[29] In addition to classical mechanical rheometry, this paper uses novel rheological techniques, diffusing wave spectroscopy[30,31] and single-particle tracking microrheometry.[31−33] Preshear upon loading of actin into the rheometer, which has been evoked to explain the discrepancy between reported values of G'_p,[19] is avoided using these two techniques. The combination of mechanical and optical measurements allow us to show that while stress relaxation via long-time reptation dominates at long times, the stress relaxation via transverse fluctuations of the polymers dominates at short times.

This paper also offers the first direct comparison between experiments and theories for semiflexible polymers. Our new rheological results allow us to discriminate between those theories. This paper reports unusual exponents for the frequency dependence of the viscoelastic modulus and the concentration dependence of the small-frequency storage modulus G'_p, which are all correctly predicted by the new curvature-stress model of semiflexible-polymer rheology. This agreement supports the curvature-stress model of viscoelasticity of solutions of semiflexible polymers at small and large frequencies.

2. Experimental Techniques

Actin Preparation. Actin was purified from rabbit skeletal muscle acetone powder by the slightly modified method of Spudich and Watt.[34] The resulting actin was gel filtered on Sephacryl S-300 HR instead of Sephadex G-150.[35] The purified actin was stored as Ca^{2+}−actin in continuous dialysis at 4 °C against daily changed buffer G (0.2 mM ATP, 0.5 mM DTT, 0.1 mM $CaCl_2$, 1 mM NaAzide, and 2 mM Tris−Cl, pH 8.0 at 25 °C).

S0024-9297(97)01775-0 CCC: $15.00
Published on Web 09/03/1998

The final actin concentration was determined by ultraviolet absorbance at 290 nm, using an extinction coefficient of 2.66 $\times 10^4$ M^{-1} cm^{-1}, and a cell path length of 1 cm. Mg^{2+}−actin filaments were generated by adding 0.1 volume of 10 − x KME (500 mM KCl, 10 mM $MgCl_2$, 10 mM EGTA, 100 mM imidazole, pH 7.0) polymerizing salt buffer solution to 0.9 volume of G-actin in buffer G, respectively. The actin used for all experiments came from the last fraction of the actin peak obtained by gel filtration.

Electron Microscopy. Actin was polymerized with KME in a volume of 100 μL, placed into a porcelain tray, and allowed to polymerize overnight at room temperature in a humidified room. Samples are fixed, embedded, and sectioned as described in Wachsstock et al.[20, 21]

Time-Resolved Fluorescence Spectroscopy. The assembly of G-actin into F-actin is monitored by fluorescence spectroscopy using the classical pyrene assay.[36] *N*-(1-Pyrenyl)-iodoacetamide (pyrene)-actin is prepared as decribed in Cooper at al.[36] Upon incorporation of G-actin into F-actin, fluorescence of tightly bound pyrene is increased. The fluorescence intensity is directly proportional to the amount of actin incorporated into filaments.

Diffusing Wave Spectroscopy and Video-Based Single-Particle-Tracking Microrheology. Details about the optical setup for DWS are given in Palmer et al.[31] Briefly, the beam from an Ar^+ ion laser operating in the single-line-frequency mode at a wavelength of 514 nm is focused and incident upon a flat scattering cell which contains the polymerized actin solution and spherical optical probes. The light multiply scattered from the solution is collected by two photomultiplier tubes (PMT) via a single-mode optical fiber with a collimator lens of very narrow angle of acceptance at its front end and a beam splitter at its back end. The outputs of the PMTs are directed to a correlator working in the pseudo-cross-correlation mode to generate the autocorrelation function $g_2(t) - 1$ from which quiescent rheological properties of the actin solutions can be calculated.

Actin is polymerized in situ for 12 h before measurement by loading the scattering cell with a solution of monomeric actin mixed with the polymerizing salt solution and a dilute suspension of monodisperse latex microspheres (Duke Scientific Corp.) of radius 0.48 μm at a volume fraction of 0.01. The scattering cell is then immediately tightly capped. We verified by both time-resolved static light scattering and time-resolved mechanical rheology that G-actin was fully polymerized into F-actin at all concentrations presented in this paper before the 12 h was complete. Using static light scattering, we verified that more than 95% of the scattering intensity in the transmission geometry was due to the microspheres, less than 5% due to the actin filament network itself. We also verified using mechanical rheology that the added latex beads did not affect the rheology of polymerized actin, representing less than 5% of the magnitude of $G'(\omega)$ and $G''(\omega)$ at all actin concentrations used in this paper. All DWS measurements are conducted at a temperature of $T = 23$ °C.

Details about our video-based single-particle-tracking microrheometer are given in Mason et al.[33] and Xu et al.[37] Briefly, a 0.96 μm diameter microsphere is imbedded into the F-actin network. Its position is tracked with ≈5−10 nm resolution by monitoring the center-of-mass displacements of the two-dimensional light intensity of the Airy figure of the particle. The rate at which our video-microscopy-based microrheometer can track particle motion is slightly smaller than the video rate of image acquisition. Therefore, the maximum frequency of viscoelastic moduli which can be probed by that technique is about 5−10 Hz. We conduct particle-tracking measurements on more than 25 individual particles. Similarly to DWS, advantages of single-particle-tracking microrheometry include the possibility to generate viscoelastic moduli without subjecting the specimen to shear, which can induce bundling and breakage of the polymers. However, unlike DWS, this technique can also generate anisotropic viscoelastic moduli and only requires extremely small sample volumes, 20 μL, as opposed to ≈1 mL for a regular rheometer and DWS. The general method used to extract $G'(\omega)$ and $G''(\omega)$ directly from MSD measurements (particle-tracking microrheology) or from $g_2(t) - 1$ via the calculated values of the MSD of the optical probes (DWS microrheology) is described in details in Palmer et al.[31]

Mechanical Rheometry. To compare our optical measurements with classical mechanical measurements, we employ a strain-controlled mechanical rheometer (ARES-100 Rheometrics, NJ) equipped with a 50 mm diameter cone and plate geometry.[38] To prevent possible evaporation effects, the cone and plate tools are enclosed in a custom-made vapor trap. The temperature of the sample is fixed at $T = 23 \pm 0.1$ °C. The linear values $G'(\omega)$ and $G''(\omega)$ of the actin solutions are measured by setting the amplitude of the perturbative oscillatory strain at $\gamma = 1\%$ and sweeping from low to high frequency. The onset of elasticity in an F-actin network is measured by monitoring the time-dependent $G'(t)$ and $G''(t)$ at a fixed frequency, $\omega = 1$ rad/s, and a fixed strain, $\gamma = 1\%$. The G-actin solution is placed between the cone and plate tools and allowed to gel in the presence of polymerizing salt for 8−12 h, prior to the measurements. The viscoelastic properties of actin solutions are found independent of time after 8−12 h at all actin concentrations used in this work.

3. Results and Discussion

This section presents the linear viscoelastic moduli of actin networks measured during gelation, the linear frequency-dependent elastic and loss moduli at equilibrium, and the concentration dependence of the small-frequency plateau modulus of pure actin filament networks. We compare our mechanical and optical results to the model of MacKintosh et al.[9](the tension-stress model) and the models of Isambert and Maggs[10] and Morse [11] (the curvature-stress model).

3.1. The Viscoelastic Nature Changes During Network Formation. The viscoelastic nature of F-actin solutions, i.e., the relative values of the elastic and loss moduli, has been the subject of much debate.[19] We show here that the rheology of F-actin depends first on the state of gelation of the actin network. Network formation from polymerized actin is extremely slow compared to the kinetics of actin polymerization itself. We measure independently the kinetics of actin self-assembly and the kinetics of onset of elasticity.

Using time-resolved fluorescence spectroscopy, we monitor the extent of actin polymerization upon addition of salt to the solution of actin monomers (G-actin). The salt screens electrostatic interactions between actin monomers, which promotes their linear aggregation into long, semiflexible polymers. Figure 1 displays the fluorescence intensity normalized by the steady state value as a function of time and initial G-actin concentration. This figure shows how rapidly this polymerization process occurs and how the kinetics of self-assembly is accelerated for increasing actin concentration. For instance, for $c = 24$ μM, it takes about 1 min to reach 95% of the steady-state value. After this short polymerizing time, actin filaments overlap as shown in Figure 2.

However, even though the onset of overlap between actin filaments is rapid, the formation of a quiescent elastic actin network is extremely slow. While it takes a few minutes for actin polymerization to be completed, it takes typically from 8 to 10 h for the elasticity of an F-actin solution to reach steady state. Figure 3 shows the time-dependent elastic and loss moduli during the gelation of polymerized actin. These time-dependent viscoelastic moduli are monitored at a fixed frequency $\omega = 1$ rad/s and a fixed small strain $\gamma = 1\%$ using a high-resolution strain-controlled rheometer. While the

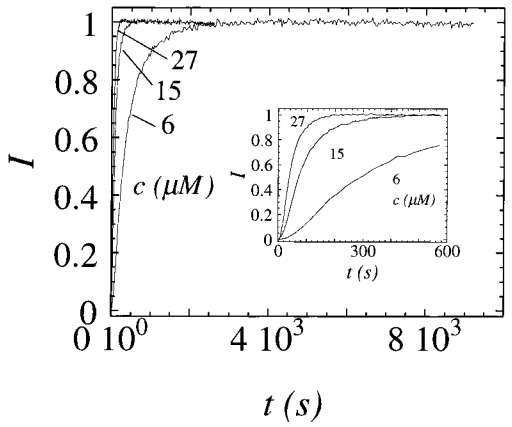

Figure 1. Evolution of the fluorescence intensity due the assembly of G-actin into F-actin upon addition of a KMEI salt as measured by time-resolved fluorescence spectroscopy. The kinetics of polymer formation is dramatically enhanced for increasing actin concentrations.

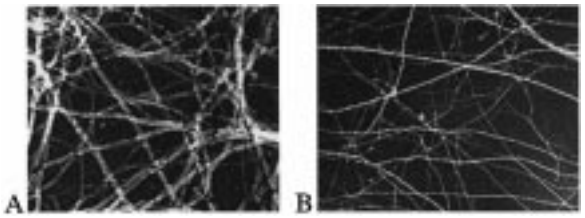

Figure 2. Electron micrograph of a 1 μM actin network. The subsections of the actin filaments are almost rigid between polymer overlaps.

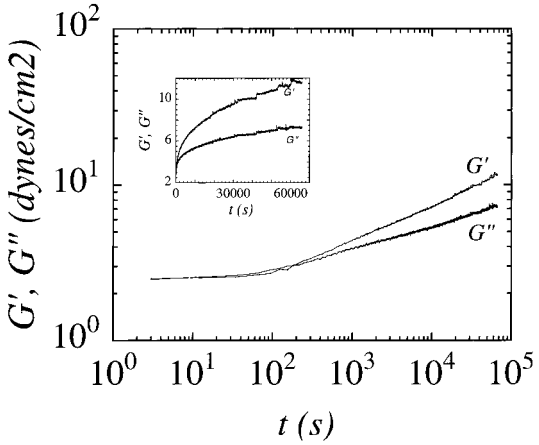

Figure 3. Evolution of elastic and storage moduli of F-actin network upon addition of salt to a 24 μM G-actin solution measured at $\omega = 1$ rad/s and $\gamma = 1\%$ using the strain-controlled mechanical rheometer. The F-actin network formation is extremely slow compared to the kinetics of actin polymerization (see Figure 1).

loss modulus slightly dominates at the earliest times of the network formation (by then the actin has already fully polymerized), the elastic modulus dominates at long times. Therefore, the viscoelastic nature of actin solutions greatly changes with the state of network formation, liquidlike at the early stage and solidlike at the late stage of gelation.

3.2. Equilibrium Viscoelastic Moduli As Measured by DWS, Single-Particle-Tracking, and Mechanical Rheometry. The description of actin rheology at equilibrium has been oversimplified. Here, we show that the viscoelastic nature of actin solutions depends not only on the state of gelation of actin (as shown above) but also on the frequency of the mechanical excitation, especially at large frequencies. After formation of an elastic network (i.e. after about 10 h), we measure the frequency-dependent viscoelastic moduli of actin networks using diffusing wave spectroscopy, single-particle-tracking microrheology, and mechanical rheometry. These instruments complement one another. Mechanical rheometry allows us to probe the effects of strain on actin rheology, to measure the small-frequency dependence of the viscoelastic moduli, and to directly compare optical and mechanical measurements. DWS allow us to probe structural and rheological heterogeneities of the actin network and to measure the high-frequency viscoelastic moduli. Particle-tracking microrheology allows us to show that a simple video-based imaging technique can be used to obtain semi-quantitative measurements of the viscoelastic moduli, at least at small frequencies.

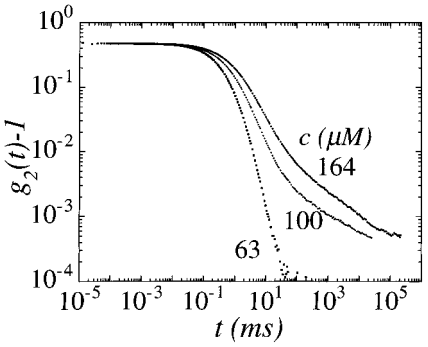

Figure 4. Autocorrelation function $g_2(t) - 1$ of the light intensity detected by the PMTs and calculated by the cross-correlator of the DWS instrument obtained after a 24-h run on F-actin networks. From these $\langle \Delta r^2(t) \rangle$ measurements, we calculate the viscoeastic properties of F-actin networks optically shown in Figure 5.

3.2.1. DWS and Particle-Tracking Measurements of Viscoelastic Moduli. Viscoelastic moduli of actin solutions are computed from the autocorrelation function $g_2(t) - 1$ of the multiply scattered light, which is transmitted through the actin gel containing the probing microspheres (see Methods section). From $g_2(t) - 1$, we compute the mean square displacement $\langle \Delta r^2(t) \rangle$ of the microspheres,[31] from which we extract the complex function G^* and the frequency-dependent viscoelastic moduli $G'(\omega)$ and $G''(\omega)$.

Figure 4 displays $g_2(t) - 1$, as detected by the PMTs and calculated by the cross-correlator of the DWS instrument at different actin concentrations. The measured autocorrelation function is displayed over a large temporal range corresponding to 10 decades, between 10^{-7} and 10^2 s. The function $g_2(t) - 1$ exhibits a decay over approximately 2 decades in time and then levels off at long times due to a partial trapping of the optical probes by the actin mesh. By collecting at least four DWS runs for each actin concentration, we checked the reproducibility of our optical measurements of $g_2(t) - 1$. Sample−aging effects are negligible, at least within 3−5 days: no significant optical and rheological changes occurred after the preparation of G-actin and immediate polymerization. At large actin concentrations, ergodicity problems can arise due to the onset of inhomogeneities in F-actin solutions. To verify ergodicity, we conducted runs on the same actin samples with the laser beam incident upon 5 different points of the face of the scattering cell. Local variations of $g_2(t) - 1$ were found to be negligible for actin concentration

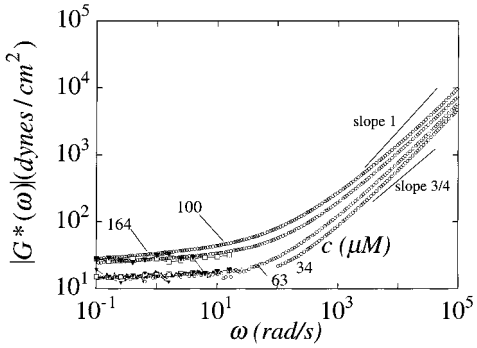

Figure 5. Complex viscoelastic modulus $|G^*(\omega)|$ obtained from DWS (closed circles), video-based single-particle-tracking measurements of $\langle \Delta r^2(t) \rangle$ (closed losanges), and mechanical rheometry (open squares). These measurements display a characteristic plateau at low frequencies an a power law increase at frequencies larger than 200 Hz, which are not measurable using classical rheometry. The high-frequency viscoelastic modulus of F-actin solutions scales such as $|G^*(\omega)| \propto \omega^{0.78\pm0.10}$, with an exponent much larger than expected for flexible polymers for which $|G^*(\omega)| \propto \omega^{1/2}$.

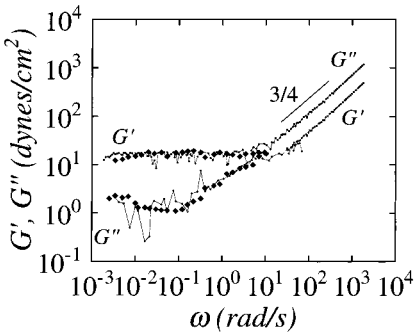

Figure 6. Linear equilibrium storage and loss moduli of actin as measured using mechanical rheometry (measured at $\gamma = 1\%$) and DWS between 10^{-3} and 10^5 rad/s for a 24 μM F-actin solution, 12 h after addition of the polymerizing salt to the G-actin solution. The storage modulus is weakly frequency dependent up to $\omega \leq 1$ rad/s. The small-frequency elastic modulus (the "plateau modulus") has a small magnitude, G'_p 14 ± 3 dynes/cm^2.

smaller than $\approx$48−60 μM, but observed to increase for increasing actin concentration.

Using the analytical framework developed in Palmer et al,[31] the macroscopic viscoelastic modulus $|G^*(\omega)|$ can be computed directly by Laplace transformation of the discrete $\langle \Delta r^2(t) \rangle$ data and is displayed in Figure 5. Each curve displays a characteristic plateau at small frequencies up to a characteristic crossover frequency, ω_ϵ, and a rapid increase of $|G^*(\omega)|$ for increasing frequency after that crossover frequency. As expected, this crossover frequency corresponds to the inverse of the characteristic time at which $g_2(t) - 1$ levels off.

One of the most remarkable features of $|G^*(\omega)|$ is its unique scaling with frequency at high-frequencies

$$|G^*(\omega)| \propto \omega^{0.78\pm0.10} \quad \text{for} \quad \omega > 200\ s^{-1} \qquad (1)$$

for $c = 24$ μM. Morse's model[11] predicts that this power law behavior reflects the finite rigidity of actin, and is a general property of semiflexible polymers. Figure 6 shows the frequency-dependent elastic and loss moduli for a 24 μM actin solution measured using mechanical rheometry and optical rheometry. Excellent agreement is observed between optical and mechanical measurements.

3.2.2. Comparison with Reported Values and Theoretical Models. Rheological measurements of the frequency dependence of the elastic and loss moduli for $\omega > 100$ rad/s are extremely limited, therefore direct comparison with published data is difficult at high-frequencies. Moreover, like stress-controlled rheometers,[19] magnetic micro-rheometers,[39] and torsion pendulums,[19,25,26] our strain-controlled rheometer can measure $G'(\omega)$ and $G''(\omega)$ only up to about 80−100 rad/s, so a direct comparison of our optical measurements with our mechanical measurements at large frequency is also precluded. The scaling $|G^*(\omega)| \propto \omega^{3/4}$ was recently observed by Gittes et al.,[40] for $c = 24$ μM using another type of particle-tracking setup. We first note that our combined mechanical and optical instruments provide for a much more extended frequency range, between 10^{-4} and 10^5 Hz, than the frequency range probed by Gittes et al.,[40] which is between 10 and 300 Hz. Taking advantage of this extended frequency range, we systematically observe the onset of a small-frequency plateau at around 10 Hz. Gittes et al. do not observe such a small-frequency plateau modulus, in disagreement with our optical and mechanical measurements and with all previous mechanical measurements.[12−28] A possible explanation for this discrepancy is that Gittes et al. conducted their measurements only 1 h after initiation of actin polymerization. As shown in section 3.1 above, it takes about 10 h for the elasticity to set in, independently of actin concentration.

Recent theoretical models predicted the high-frequency dependence of $|G^*(\omega)|$. In addition to the fact that the measurement of the frequency dependence of $|G^*(\omega)|$ provides us with a much more rigorous test of current dynamical models of actin gel dynamics, the high-frequency regime also offers new insight into the local dynamics of actin filaments inside their confinement tube. Morse[11] has recently constructed a model, which specifically describes the rheological behavior and dynamics of semiflexible polymers in solution. This model predicts that at large frequencies, $|G^*(\omega)| \propto \omega^\alpha$ with $\alpha = {}^3/_4$, in agreement with our DWS measurements. This exponent α is much larger than the one describing the large-frequency behavior of flexible polymer in a Θ solvent, for which $\alpha = {}^1/_2$.[8] For flexible Zimm chains, for which hydrodynamic interactions are taken into account, $\alpha = {}^2/_3$,[8] which is closer to the exponent that we obtain with actin solutions.

Equation 1 also predicts that at large frequencies, the loss modulus becomes larger than the storage modulus. In the power-law regime, $G^*(\omega) \propto (i\omega)^\alpha$, where $\alpha = {}^3/_4$, therefore $G''/G' = \tan(\pi\alpha/2) \approx 2.41$ (phase shift $\delta \approx 67.5°$), as observed in Figure 6. As a conclusion, F-actin solutions are viscoelastic solids ($G' > G''$) at small frequencies and viscoelastic liquids ($G'' > G'$) at large frequencies.

3.3. Magnitude and Concentration Dependence of Elastic Modulus. 3.3.1. Scaling with Concentration. In Figure 7, we plot the low-frequency elastic plateau modulus G'_p, which is evaluated at $\omega = 1$ s^{-1} (i.e., $G'_p \equiv G'(\omega = 1$ rad/s)), as a function of actin concentration c. Figure 7 shows both mechanical and optical measurements of G'_p, which are in agreement. The magnitude of the elastic plateau is $G'_p \approx 14 \pm 3$ dynes/cm^2 for a 24 μM actin solution. The concentration $c = 24$ μM is chosen here because it has become the standard concentration to compare values in different labs and to study the effects of regulating proteins on

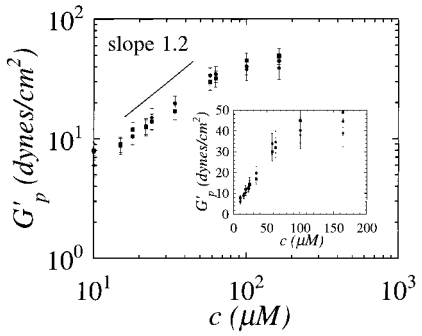

Figure 7. Low-frequency elastic plateau modulus G'_p as a function of actin concetration measured using mechanical rheometry (circles), DWS (squares), and particle-tracking microrheology (losanges). We arbitrarily defined the "plateau modulus" as $G'_p \equiv G'(\omega = 1$ rad/s). For concentrations $c < 63$ μM, the data is fit by a power law of c; we find $G'_p \propto c^{1.2\pm0.2}$, which is in agreement with Morse's model. This figure shows saturation in the measured G'_p at concentrations $c > 63$ μM, which may indicate the onset of local liquid crystalline ordering at high actin concentration.

F-actin rheology.[16−21,28] For concentrations $c \leq 63$ μM, G'_p can be fit by an effective power law of c as

$$G'_p(c) \propto c^{1.2\pm0.2} \quad \text{for} \quad c \leq 50-63\ \mu\text{M} \qquad (2)$$

3.3.2. Comparison with Published Data and Theoretical Models. Few systematic studies of the concentration dependence of the elastic plateau modulus are available. Janmey and co-workers have reported $G'_p(c) \propto c^{2.2}$ for 6.6 μM $< c <$ 50 μM with a magnitude between $G'_p \approx 150$ dynes/cm^2 and $G'_p \approx 5000$ dynes/cm^2, respectively.[16−19] Our mechanical and optical measurements of the amplitude of the plateau modulus, which agree with one another to within 20%, yield values that are between 15 and 350 times smaller and exhibit a much weaker concentration dependence. Our measurements are, however, in good agreement with those published in refs 20−23 at least for $c = 24$ μM.

We find excellent agreement between our measured concentration dependence of the plateau modulus, $G'_p \propto c^{1.2\pm0.2}$, and that predicted by the curvature-stress model,[10,11] $G'_p \propto c^{1.4}$. We can further test the curvature-stress model[11] by comparing the measured and calculated magnitudes of the plateau modulus. The curvature-stress model predicts $G'_p = 7k_BT\rho/5l_e$. Here, ρ is the contour length of F-actin per unit volume, which is given by $\rho = cl_AN_A \cong 38.5$ μm^{-2} when c = 24 μM, N_A is the Avogadro number, and $l_A = 2.75$ nm is the curvilinear length of a G-actin monomer.[1] Since a direct measurement of the entanglement length l_e is difficult, we estimate it using a geometric argument given in Morse,[11] $l_e \cong l_p(\rho l_p^2)^{-2/5} \approx 0.32-0.38$ μm with a persistence length $l_p = 5-15$ μm. We find $G'_p \approx 7k_BT\rho/5l_e \approx 7$ dynes/cm^2, in fair agreement with our measured plateau modulus.

Another important assumption underlying the curvature-stress model is that the entanglement length l_e obtained from the measured plateau modulus as $l_e \cong 7k_BT\rho/5G'_p$ is smaller than the polymer contour length and larger than the mesh size.[11] Using the measured value of the plateau modulus $G'_p \cong 15$ dynes/cm^2, we estimate $l_e \approx 0.15$ μm, which is close to that predicted from geometric arguments (see above). As assumed in the curvature-stress model,[11] we find that the entanglement length is smaller than the average F-actin contour length, since $L \approx 10-25$ μm, and is on the order of the average mesh size $\xi = 0.15$ μm for $c = 24$ μM, estimated from geometric arguments, $\xi \cong \rho^{-1/2} \approx 0.15$ μm.

We now compare the measured concentration dependence and magnitude of the plateau modulus with the predictions of the tension-stress model.[9] The tension-stress model predicts a plateau modulus $G'_p \cong k_BTl_p^2/\xi^2l_e^3$, which ranges from $G'_p \approx 10^3$ dynes/cm^2 to $G'_p \approx 10^4$ dynes/cm^2 for $l_e \approx 0.35$ μm and $l_e = 0.15$ μm, respectively (using $\xi \approx 0.15$ μm and $l_p \approx 5$ μm), which are both much larger than the measured value of the plateau. However, the amplitude of G'_p predicted by the tension-stress model is highly dependent on the evaluation of l_e. If we use the estimate of l_e based on a heuristic argument which yields an entanglement length that is about twice the tube diameter $D_e \approx 0.5$ μm, $l_e \approx 1$$\mu$m, then we find $G'_p \approx 50$ dynes/cm^2, which is still slightly too large. This disagreement worsens at actin concentrations larger than $c > 24$ μM since, according to the tension-stress model, G'_p depends strongly on concentration, $G'_p \propto c^{2.2}$, in disagreement with our measurements. Finally, we note that in disagreement with the recent predictions of Maggs,[41] we do not observe the presence of a second plateau modulus at large frequencies.

3.4. Linear Rheology of the Liquid Crystalline Phase. Past an actin concentration of about 48−60 μM, we observe the onset of birefringence (not shown here). We also observe the onset of nonergodicity in our multiple-light scattering measurements. This transition between an isotropic phase and an anisotropic nematic-like phase has been reported previously for actin.[42] Here, we report the linear rheological properties of the nematic phase of actin. As shown in Figure 5, we observe that the qualitative shape of the frequency-dependent viscoelastic modulus is unchanged compared to that of isotropic solutions of actin. In particular, we observe that the viscoelastic modulus varies with frequency as $|G^*(\omega)| \propto \omega^{0.85\pm0.05}$. We also observe that the onset of the plateau modulus occurs at decreasing frequencies.

The persistence of the power-law behavior across the isotropic−nematic phase transition line is expected in view of the underlying physics predicting $|G^*(\omega)| \propto \omega^{3/4}$. Since this behavior stems from the rapid dynamics of relaxation of the stress at length scales smaller than the entanglement length, the large length scale nematic ordering of the actin filaments should only affect the magnitude and concentration dependence of the small frequency plateau modulus and not the high-frequency behavior. Since the diameter of the tube confining each polymer becomes smaller for increasing concentrations, the onset of this power law behavior occurs at smaller frequencies. Accordingly, the entanglement time, the time at which entanglement effects become important, decreases in magnitude for increasing concentrations.

One of the most remarkable rheological features of the nematic phase of long semiflexible polymers is that the plateau modulus becomes independent of concentration. As shown in Figure 7, for increasing concentrations, G'_p saturates at around 60 μM to a value 30−40 dynes/cm^2. This observation cannot be explained straightforwardly by current theories.

3.5. Origin of the Stress in Concentrated Solutions of Semiflexible Polymers. In view of the success of the curvilinear-stress model of Isambert and Maggs and Morse in correctly predicting the linear shear rheology of solutions of semiflexible polymers, including

the frequency dependence of the viscoelastic modulus, the concentration dependence, and the magnitude of the small-frequency plateau modulus, we can use its underlying ideas to gain insight into the dynamics and rheology of these systems. The small-frequency stress has two origins: the curvature stress and the orientational stress.[11] In the present case of long semiflexible actin filaments, the former dominates at all time scales; the latter would become important for shorter, more rodlike semiflexible polymers.[11] This curvature stress originates from the forces which attempt to suppress transverse deformations of the initial tube inside which each polymer is confined, hence the name curvature-stress model. At large frequencies, the stress arises from the bending modes of the polymers at length scale smaller than the entanglement length.[11] Morse's model predicts that the plateau modulus is independent of the length of polymers. We leave to future work the study of the effect of length on the viscoelastic properties of actin solutions.

The curvature-stress model can be contrasted with the earlier tension-stress model of MacKintosh et al.,[9] which assumes that the elastic stress arises from the forces generating tangential stretching and compression of the subsections between entanglements, which prevent the growth or reduction of the transverse fluctuations of wavelength smaller than the entanglement length. The tension-stress model fails to describe the viscoelasticity of actin solution at small frequencies: the model predicts a strong concentration dependence of the small-frequency plateau modulus, in disagreement with our DWS, mechanical, and particle-tracking microrheological measurements. However, the mechanism invoked by the tension-stress model can describe the viscoelasticity of actin solutions at large frequencies. With the same physics as in the tension-stress model, Morse predicts the scaling $|G^*(\omega)| \propto \omega^{3/4}$, which we observe. The tension-stress model should be a good starting point to describe the small-frequency rheology of cross-linked networks of semiflexible polymers since the underlying physics of the model is that of a chemically cross-linked network (Morse, private communication), such as F-actin cross-linked by α-actinin. In a separate paper,[31] using the large bandwidth of DWS microrheology, we showed that the high-frequency behavior of cross-linked actin network is similar to that of un-cross-linked actin networks.

4. Conclusions

This paper reports a systematic experimental study of the rheology of model semiflexible polymers (actin filaments), over extended ranges of polymer concentrations and frequencies of deformation. Careful actin preparation as well as a combination of mechanical and optical measurements allow us to provide a more complete dataset and avoid spurious results. In particular, we avoid contamination of actin with capping and cross-linking proteins which can dramatically modify actin rheology. We observe surprisingly good agreement between optical and mechanical measurements, at least over the limited frequency range probed by our mechanical rheometer. We show that the viscoelastic nature of actin networks depends strongly on the frequency of shear deformation and the extent of gelation of the actin network.

Both mechanical and optical instruments measure a small magnitude for the plateau modulus, which has also a weak concentration dependence, $G'_p \propto c^{1.2\pm0.2}$. At high frequencies probed by DWS, the viscoelastic modulus is shown to increase with an unusual power law of frequency, $|G^*(\omega)| \propto \omega^{0.78\pm0.10}$, which reflects the finite rigidity of actin.

These new systematic measurements are in disagreement with the tension-stress model of MacKintosh et al., which assumes that the small-frequency plateau modulus originates from forces preventing the compression and of chain segments between entanglements. Our measurements are however in remarkable agreement with the curvature-stress model of Morse and Isambert and Maggs, which assumes that this plateau modulus stems from the forces that prevent tube bending. Our study offers a baseline for future studies on the effect of cross-linking, capping, and severing proteins on F-actin rheology, all of which can serve as model systems of semiflexible polymers with tunable viscoelastic properties. Our report here also presents the first use of DWS to uncover new polymer physics at large frequencies.

Acknowledgment. We acknowledge D. Morse and A. Maggs for helpful discussions about the physics of semiflexible polymers. We are especially grateful to T. D. Pollard for his help in actin preparation, which is the key to any meaningful study of their physical properties, and for his insight into actin in general. We thank K. Rufener and T. G. Mason for their help in the DWS measurements as well as S. C. Kuo for fruitful conversations. D.W. acknowledges financial support from the National Science Foundation, Grants DMR 9623972 (CAREER), CTS 9502810, and CTS 9625468.

References and Notes

(1) Alberts, B.; Bray, D.; Lewis, J.; et al. *Molecular biology of the cell*; Garland Publishing: 1994.
(2) Burlacu, S.; Janmey, P. A.; Borejdo, *J. Am. J. Physiol* **1992**, *262*, C569.
(3) Gittes, F.; Mickey, B.; Nettleton, J.; et al. *J. Cell Biol.* **1993**, *120*, 923.
(4) Isambert, H.; Venier, P.; Maggs, A. C.; et al. *J. Biol. Chem.* **1995**, *270*, 11437.
(5) de Gennes, P.-G. *Scaling concepts in polymer physics*; Cornell University Press: New York, 1979.
(6) Ferry, J. D. *Viscoelastic properties of polymers*; John Wiley and Sons: New York, 1980.
(7) Flory, P. J. *Principles of polymer chemistry*; Cornell University Press: New York, 1953.
(8) Doi, M.; Edwards, S. F. *The theory of polymer dynamics*; Clarendon Press: Oxford, England, 1989.
(9) Macintosh, F. C.; Kas, J.; Janmey, P. A. *Phys. Rev. Lett.* **1995**, *75*, 4425.
(10) Isambert, H.; Maggs, A. C. *Macromolecules* **1996**, *29*, 1036.
(11) Morse, D. Submitted for publication in *Macromolecules*, 1997.
(12) Muller, O.; Gaub, H.; Barmann; et al. *Macromolecules* **1991**, *24*, 3111.
(13) Haskell, J.; Newman, J.; Selden, L. A.; et al. *Biophys. J.* **1994**, *66*, A196.
(14) Newman, J.; Zaner, K.; Schick, K.; et al. *Biophys. J.* **1993**, *64*, 1559.
(15) Hvidt, S.; Heller, K. In *Polymers networks and gels*; Burchard, W., Ross-Murphy, S., Eds.; Elsevier: London, 1990; p 195.
(16) Janmey, P. A. Hvidt, S.; Peetermans, J.; et al. *Biochemistry* **1988**, *88*, 8218.
(17) Janmey, P. A.; Hvidt, S.; Lamb, J.; et al. *Nature* **1990**, *345*, 89.
(18) Janmey, P. A.; Euteneuer, U.; Traub, P.; et al. *J. Cell Biol.* **1991**, *113*, 155.
(19) Janmey, P. A.; Hvidt, S.; Käs, J.; et al. *J. Biol. Chem.* **1994**, *269*, 32503.

(20) Wachsstock, D.; Schwarz, W. H.; Pollard, T. D. *Biophys. J.* **1993**, *65*, 205.
(21) Wachsstock, D.; Schwarz, W. H.; Pollard, T. D. *Biophys. J.* **1994**, *66*, 801.
(22) Sato, M.; Leimbach, G.; Schwarz, W. H.; et al. *J. Biol. Chem.* **1985**, *260*, 8585.
(23) Sato, M.; Schwarz, W. H.; Pollard, T. D. *Nature* **1987**, *325*, 828.
(24) Zaner, K. S.; Stossel, T. P. *J. Cell. Biol.* **1982**, *93*, 987.
(25) Zaner, K. S.; Stossel, T. P. *J. Biol. Chem.* **1983**, *258*, 11004.
(26) Zaner, K. S.; *J. Biol. Chem.* **1986**, *261*, 7615.
(27) Zaner, K. S.; Hartwig, J. H. *J. Biol. Chem.* **1988**, *263*, 4532.
(28) Xu, J.; Wirtz, D.; Pollard, T. D. *J. Biol. Chem.* **1998**, *273*, 9570.
(29) Casella, J. F.; Barron-Casella, E. A.; Torres, M. A. *Cell Motil. Cytoskeleton* **1995**, *30*, 164.
(30) Weitz, D. A.; Pine, P. J. In *Dynamic Light Scattering*; Wyn, B., Ed.; Oxford University Press: Oxford, England, 1993.
(31) Palmer, A.; J. Xu., Wirtz, D. *Rheol. Acta* **1998**, *37*, 97.
(32) Mason, T. G.; Ganesan, K.; van Zanten, J. V.; Wirtz, D.; Kuo, S. C. *Phys. Rev. Lett.* **1997**, *79*, 3282.
(33) Mason, T. G.; Dhople, A.; Wirtz, D. In *Statistical mechanics in physics and biology*; Wirtz, D., Halsey, T. C., Eds.; MRS: Pittsburgh, PA, 1997; Vol. 463, p 153.
(34) Spudich, J. A.; Watt, S. *J. Biol. Chem.* **1971**, *246*, 4866.
(35) MacLean-Fletcher, S. D.; Pollard, T. D. *J. Cell. Biol.* **1980**, *85*, 41.
(36) Cooper, J. A.; Walker, S. B.; Pollard, T. D. J. *Muscle Res. Cell Motil.* **1983**, *4*, 253−262.
(37) Xu, J.; Viasnoff, V.; Wirtz, D. *Rheol. Acta*, in press 1998.
(38) Mason, T. G.; Dhople, A.; Wirtz, D. *Macromolecules* **1998**, *31*, 3600.
(39) Ruddies, R.; Goldmann, W. H.; Isenberg, G.; et al. *Biochem. Soc. Trans.* **1993**, *21*, 37S.
(40) Gittes, F.; Schnurr, B.; Olmsted, P. D.; et al. *Phys. Rev. Lett.* **1997**, *79*, 3286.
(41) Maggs, A. C. *Phys. Rev.* E **1997**, *55*, 7396.
(42) Coppin, C. M.; Leavis, P. C. *Biophys. J.* **1993**, *63*, 794.

MA9717754